The Wave Field around DEXA Devices and Implications for Coastal Protection

Zanuttigh, Barbara; Angelelli, Elisa; Castagnetti, Mirko; Kofoed, Jens Peter; Martinelli, Luca; Clausen, Lars

Published in:
9th ewtec 2011

Publication date:
2011

Document Version
Publisher's PDF, also known as Version of record

The wave field around DEXA devices and implications for coastal protection

Barbara Zanuttigh[1], Elisa Angelelli[2], Mirko Castagnetti[3], Jens Peter Kofoed[4], Luca Martinelli[5], Lars Clausen[6]

DICAM – University of Bologna,
Viale Risorgimento 2, 40136 Bologna, Italy
[1] barbara.zanuttigh@unibo.it
[2] elisa.angelelli4@unibo.it
[3] mirko.castagnetti2@unibo.it

Department of Civil Engineering, University of Aalborg,
Sohngaardsholmsvej 57, 9000 Aalborg, Denmark
[4] jpk@civil.aau.dk

IMAGE - University of Padova,
Via Ognissanti 39, 35129 Padova, Italy
[5] luca.martinelli@unipd.it

DEXAWAVE Energy ApS
Enghaven 49, 7500 Holstebro, Denmark
[6]dexadk@gmail.com

***Abstract* – The purpose of this paper is to examine the hydrodynamics around floating wave energy converters (f-WECs). In particular, the paper considers the case of the f-WEC of the Wave Activated Body type, named DEXA. Based on 3D wave experiments in the Laboratory of the Aalborg University (DK), the modified wave field around a wave energy farm (composed by three 1:60 scale models) and around a single device (1:30 scale model) is investigated. Specific results include wave reflection, wave transmission and wave disturbance around the device. The results are examined considering scale effects, influence of wave length and wave steepness.**

***Keywords*— hydrodynamics, wave energy converter, wave farm, transmission coefficient, coastal protection, DEXA, experiments.**

Nomenclature

b	model width
d	water depth
h_I	ratio between H_I at different scales
h_R	ratio between H_R at different scales
h_T	ratio between H_T at different scales
H_I	incident wave height
H_{m0}	significant wave height (frequency domain)
H_R	reflected wave height
H_s	significant wave height (time domain)
H_T	transmitted wave height
K_D	dissipation coefficient
K_R	reflection coefficient
K_T	transmission coefficient
l	model length
l/L_p	dimensionless model length
L_p	peak wave length
s	peak wave steepness
s_f	sample frequency (20 Hz)
T_p	peak period
T_s	significant period
$\Delta\theta$	Change in the wave direction
θ_I	Main direction of incident waves
θ_T	Main direction of transmitted waves

I. INTRODUCTION

At present, erosion and flood are serious threats for coastal areas and the set-up of defence technologies able to cope with sea level rise and increased storminess induced by climate change represent a great challenge.

Due to their adaptability to sea level changes and to the absence of piling-up, near-shore floating structures can be a smart defence solution. Their effectiveness however is limited to mild wave climates [1].

Until now, only floating breakwaters were used to protect the beaches. An innovative and sustainable way to combine coastal protection and energy production may be the installation of farms of floating Wave Energy Converters (f-WECs), which is under analysis within the THESEUS project (www.theseusproject.eu).

This study addresses the DEXA f-WEC (www.dexawave.com). which is a device that belongs to the Wave Activated Body (WAB) type. Preliminary tests showed that for device length to wave length ratio close to 1, DEXA is very effective [2]. This behaviour allows to produce energy

also when the sea conditions are not extreme (i.e. when the wave heights are not particularly high) resulting in more energy production throughout the yearly wave climate.

Currently, in the literature there are few contributions on the hydrodynamics induced by f-WECs and consequences for coastal defence. Among the others, an experimental study on a scaled model of the Wave Dragon (www.wavedragon.net) showed that wave transmission is particularly affected by heaving motions of the device [3]. This physical study on a single device was the basis for analysing the wake effects induced by multiple devices by means of detailed numerical simulations [4].

This paper first presents new tests carried out on a wave farm.

Fig. 1 – The DEXA concept (www.dexawave.com)

The hydrodynamics around a single device and a farm of DEXA devices is described, based on wave basin experiments at Aalborg University. Two types of models were considered: one device in 1:30 scale and three devices in 1:60 scale. The performance of the models was analysed under a variety of irregular wave attacks. The effect of a real mooring system was also considered.

Specific objectives of this paper are:

- to fully describe the hydrodynamic field around the devices, in terms of wave disturbance, wave reflection and wave transmission;
- to verify the dependence of wave transmission on the dimensionless model length and wave steepness;
- to provide guidelines for DEXA design optimisation;
- to estimate scale effects.

The paper first describes the facility and the tests, including the models, the mooring system and the equipment. The tested irregular wave conditions and the types of measurements are also provided. Main outcomes of the tests carried out on the single and the multiple devices are summarised, focusing on wave transmission and reflection. Changes of wave direction and wake effects are also investigated. Finally, a comparison among obtained data at different scales is carried out.

II. DESCRIPTION OF THE FACILITY

The hydrodynamic tests were performed in the directional wave basin of the Hydraulics and Coastal Engineering Laboratory at Aalborg University, DK. The basin is 15.7 m long (waves direction), 8.5 m wide and 1.5 m deep. The wave generator is a snake-front piston type composed of 10 actuators with stroke length of 0.5 m, enabling generation of short-crested waves. The software used for controlling the paddle system is AwaSys developed by the same laboratory [5]. Regular and irregular long and short crested waves with peak periods up to approximately 2.5 seconds, oblique 2D and 3D waves can be generated with good results.

Passive wave absorption is carried out. A 1:4 dissipative beach made of concrete and gravel with D_{50}=5 cm is placed opposite to the wave maker.

The sidewalls are made of crates (1.21x1.21 m, 0.70 m deep).

III. DESCRIPTION OF THE MODELS

The DEXA device (Fig. 1) consists of two rigid pontoons with a hinge in between, which allows each pontoon to pivot in relation to the other. The draft is such that at rest the free water surface passes in correspondence of the axis of the four buoyant cylinders. The Power Take-Off (PTO) system consists of a low pressure power transmission technology and is placed close to the centre of the system, in order to maximise the stabilisation force [2].

In the laboratory, the following two types of scale models in Froude similitude were tested.

- Small DEXA model (1:60 scale). It is 0.95 m long and 0.375 m wide (perpendicularly to wave propagation). The model is composed by two parts, which consist of two cylindrical floaters joint through two wooden legs (Fig 2). An elastic resistant strip is placed in between the pontoons in order to connect them. Three models of this type were available to carry out experiments on the effects induced by a wave farm. The total weight of each model is 3.30 kg. These models do not carry PTO systems or measurement instrumentations on board
- Big DEXA model (1:30 scale). The model (Fig. 3) is 2.10 m long (cross-shore) and 0.81 m wide (long-shore). The device weighs 23 kg and the PTO system weighs 10 kg, for a total system weight of 33 kg.

  The PTO system (view in Fig. 4) consists of a metal bar with an elongated hole, a wire welded at the two ends of the hole and a small electric engine with a wheel. The bar is connected to one half of the device through the wheel and to the other half through a load cell (strain gauge equipped “bone”, 10 mm thick). The wire is coiled around the wheel that is forced to rotate while translating along the bar hole. The rigidity of the PTO is modified by varying the resistance of the wheel to rotation and therefore the current in the engine, so that the body rigidity is changed (totally it is possible to set up 17 rigidities).

The mooring system of the model, both in 1:60 and 1:30 scales, belongs to the “spread type” [7]. It consists of four steel chains, 1.5 m long for small models and 3.0 m long for the big model. Each chain is fixed to the bottom with heavy anchors and is linked to the device at the fairlead point in the middle of the legs by means of a resistant plastic strip (Fig. 5). The weight of the anchors is 3 kg for 1:60 scale models and 30 kg for the big model.

Once the weight per length unit of the chain is chosen (0.25 kg/m for 1:60 scale models and 1.0 kg/m for the bigger one), the design procedure of mooring systems is performed by means of the catenary equations [8]. This procedure is specifically aimed at defining s_c - which is the length of the chain portion raised from the bottom - and x_c -which is the projection of s_c on the floor. The design criterion is that x_c should be approximately 1/3 of the total chain length. Values of x_c and s_c are shown in Figure 4.

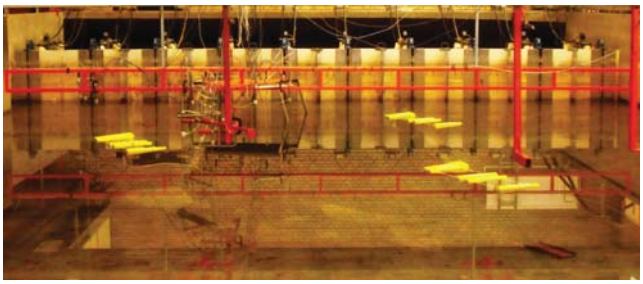

Fig. 2 – Wave energy farm with 1:60 scale models.

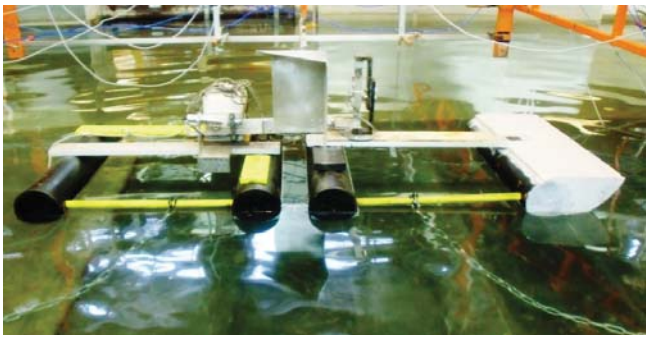

Fig. 3 - 1:30 scale model of DEXA with spread mooring.

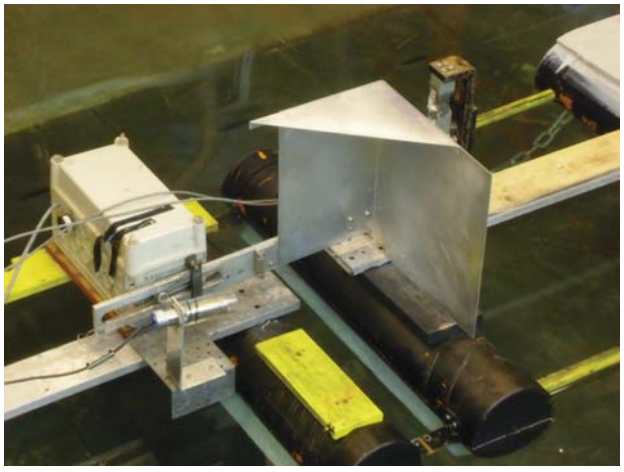

Fig. 4 – View of the PTO system.

IV. DESCRIPTION OF TESTED CONFIGURATIONS

Two test configurations were adopted in order to evaluate more accurately the behaviour of one or more devices, singularly or placed in a wave farm. Such configurations can be synthesised as follows:

1- Configuration A, wave farm (Fig.6), for investigating the changes in hydrodynamic field due to the mutual interaction of more than one device. Along the first farm line (towards the wavemaker), two models were deployed (device nr. 1 and 2, Fig. 6), with a 3.10 m wide central gap in between. In order to simulate the presence of the second farm line, a third model (nr.3) was placed just behind the gap. The water depth d_1 equals 0.3 m.

2- Configuration B, single device (Fig. 7), for assessing possible scale effects in the hydrodynamics around the big DEXA model. The water depth d_2 equals 0.60 m.

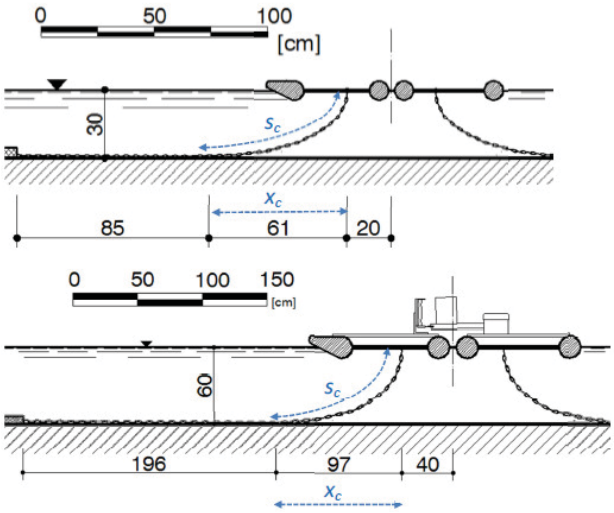

Fig. 5 – Cross section with the spread mooring system of the small models (above) and of the big model (below).

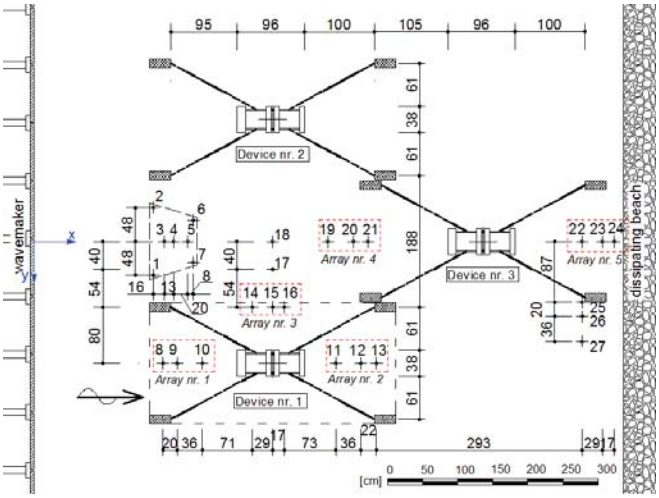

Fig. 6 Tested configuration A

V. MEASUREMENTS

The hydrodynamic measurements were performed by using in the basin a number of resistive Wave Gauges (WGs), which give the instantaneous value of the water depth. All data were simultaneously acquired at the sample frequency of 20 Hz by means of WaveLab, a software developed by Aalborg

University [9]. This software allowed also to automatically perform the calibration procedure.

A. Hydrodynamic measurements for 1:60 scale tests.

In total, 27 WGs in the basin are used (Fig. 6).

WGs allow to completely describe the hydrodynamic field in the basin by means of the water elevation time series. Values of H_s and T_s can be determined through the zero-down-crossing procedure in time domain for every WG.

The first seven WGs nr. 1-7 are deployed into a front WGs array in order to evaluate the incident and reflected wave spectra, H_{m0}, T_p and to carry out the estimation of the directional wave spectrum through the Bayesian Directional Method (BDM) [10].

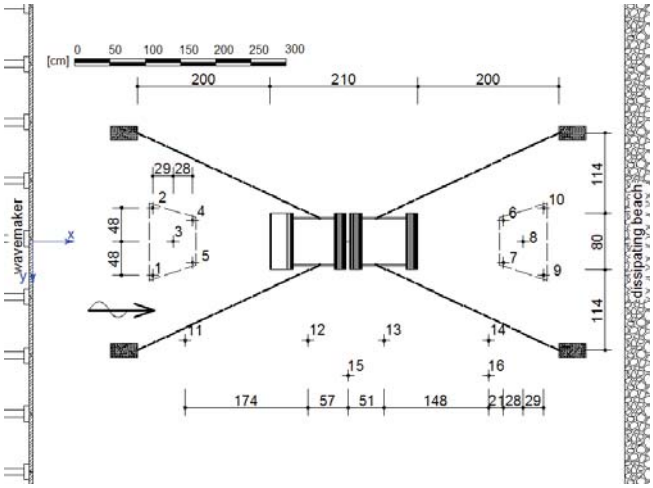

Fig. 7 Tested configuration B

Figure 5 also shows five groups of three WGs, which are necessary to calculate H_I and H_R both in front of and behind the small models:

- WGs nr 8-10 are placed in front of the device nr. 1, along the first line of the wave farm; these WGs compose Array nr. 1;
- WGs nr 11-13, placed behind the device nr. 1, correspond to Array nr. 2;
- WGs nr. 14-16 on the side of the device nr 1 compose Array nr. 3;
- WGs 19-21, just in front of the device nr. 3 composing the second line of the wave farm, correspond to Array nr. 4;
- WGs 22-24 are placed in front of the beach and behind the device nr. 3; these WGs compose Array nr. 5.

Data acquired from these Arrays were processed by means of the Mansard and Funke's method [11] to separate incident and reflected wave height.

B. Hydrodynamic measurements for 1:30 scale tests.

In this configuration, 16 WGs are used (Fig. 7). Two arrays of 5 WGs are placed in front of and behind the device (respectively front and back Array), to evaluate the incident and reflected wave spectra, H_{m0} and T_p. For such WGs arrays, the estimation of directional wave spectrum by the BDM analysis is also carried out.

VI. Tested wave conditions

Preliminary tests on big DEXA model showed that wave transmission coefficient K_T and efficiency η tend to decrease and increase respectively with increasing the dimensionless length l/L_p [12]. These new wave attacks have been therefore selected to assess more in depth the dependence of K_T on l/L_p, in order to provide an overview of the device capability of littoral protection.

Wave States (WSs) in Tab. I (1:60 scale tests) are perfectly in scale with the ones given in Tab. II (1:30 scale tests), with exception of WSs nr. 1 and 2 in Tab. II that were not carried out in 1:60 scale due to wavemaker limitations in reproducing small waves.

All tested conditions correspond to irregular waves characterised by a Jonswap spectrum (peak enhancement factor 3.3). Each test lasted for 30 minutes.

TABLE I
WAVE ATTACKS FOR 1:60 SCALE TESTS

WS	H_s [m]	T_p [s]	WS	H_s [m]	T_p [s]
1	0.05	0.74	**5**	0.067	1.01
2	0.05	0.84	**6**	0.067	1.37
3	0.05	1.01	**7**	0.083	1.01
4	0.05	1.37	**8**	0.083	1.37

TABLE II
WAVE ATTACKS FOR 1:30 SCALE TESTS

WS	H_s [m]	T_p [s]	WS	H_s [m]	T_p [s]
1	0.067	1.05	**6**	0.100	1.94
2	0.067	1.19	**7**	0.133	1.43
3	0.100	1.05	**8**	0.133	1.94
4	0.100	1.19	**9**	0.167	1.43
5	0.100	1.43	**10**	0.167	1.94

VII. Results for 1:60 scale tests

A. Transmission coefficient

The amount of transmitted wave motion can be synthetically expressed by means of the transmission coefficient, whose definition is here recalled for convenience:

$$K_T = \frac{H_T}{H_I} \qquad (1)$$

where H_I is the significant incident wave height H_{m0} and H_T is the significant transmitted wave height.

Based on eq (1), four values of K_T are used in the following:

- K_{T1} is calculated between Array nr. 1 and Array nr. 2. It represents the transmission coefficient of the device placed in the first farm line.
- K_{T2} represents the overall transmission of the first farm line. H_I is the H_{m0} derived from Array nr. 1, whereas H_T is H_{m0} calculated through a weighted average between Array nr. 2 and Array nr. 4. The weights are given by the length

along which the K_T derived from the Array is supposed to be constant. By assuming the axial symmetry of the basin and of hydrodynamics, the weights assigned to Arrays nr. 2 and 4 are respectively the widths of the device (0.375 m) and the extent of the central gap (3.10 m).

- K_{T3} represents the transmission coefficient induced by the device placed along the second farm line. H_I and H_T are derived respectively from the Arrays nr. 4 and nr. 5.
- K_{T4} is the transmission coefficient behind the second farm line. H_I is derived from the Array nr. 1 whereas H_T is calculated through a weighted average between Array nr. 2, 4 and 5. The axial symmetry in the basin is assumed and the weights for the average are given by the lengths along which H_T is supposed to be constant. Behind the devices nr. 1 and 2, H_T is the H_{m0} derived from Array nr. 2, whereas H_T equals H_{m0} at the Array nr. 5. The weights for these values are represented by the device widths (0.375 m). In the spaces among the devices along the y axis, H_T is the H_{m0} derived from Array nr. 4 and the weights are the widths of the spaces (1.36 m).

Wave transmission coefficients are synthesised in Tab. III for all tested wave conditions.

A great amount of wave motion is transmitted behind a single device and behind the farm since values of K_T are always above 0.75, the lower values being correspondent to the lower waves.

Figure 7 shows the dependence of K_{T1} - K_{T4} on l/L_p, where L_P is the peak wave length of the incident wave derived by Mansard and Funke's analysis at Array nr. 1.

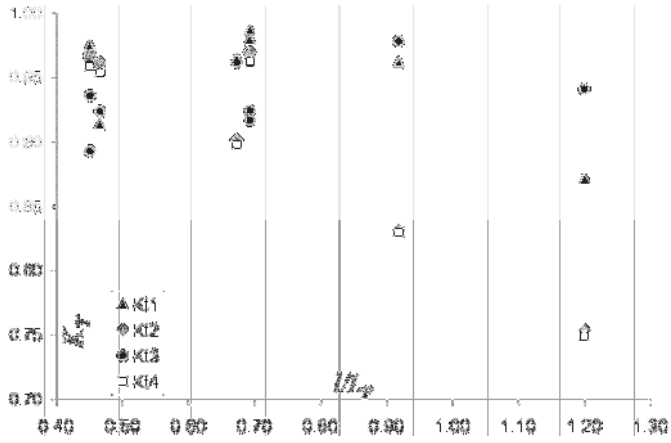

Fig. 8 K_{T1}, K_{T2}, K_{T3} and K_{T4} against l/L_p.

TABLE III
AVERAGE K_{T1}, K_{T2}, K_{T3} AND K_{T4} FOR 1:60 SCALE TESTS

	WSs							
	1	**2**	**3**	**4**	**5**	**6**	**7**	**8**
K_{T1}	0.87	0.96	0.97	0.98	0.98	0.91	0.99	0.96
K_{T2}	0.75	0.83	0.90	0.97	0.97	0.96	0.97	0.97
K_{T3}	0.94	0.98	0.96	0.94	0.92	0.92	0.92	0.89
K_{T4}	0.75	0.83	0.90	0.96	0.96	0.95	0.96	0.96

All K_T data sets in Figure 8 show a well dependence on l/L_p and have their maxima when l/L_p is around 0.70. From this value, they tend to decrease with increasing l/L_p (this tendency is a bit more marked for K_{T1}, K_{T2} and K_{T4}) and their minima are achieved when l/L_p=1.20.In particular, the trends of K_{T2} and K_{T4} have to be studied to provide a better description of the wave transmission, being K_{T1} and K_{T3} not particularly representative of the transmitted amount of wave height. In Figure 7, data sets of K_{T2} and K_{T4} almost linearly decreases with increasing l/L_p (their minima are reached when l/L_p is greater than 1.0), showing a strong dependence on l/L_p.

It can be also noticed that values and trends of K_{T4} and K_{T2} are almost equal, although the values of K_{T4} are slightly lower and the higher the values of l/L_p the smaller the differences. Therefore the mean wave transmission behind the farm is not significantly affected by the presence of the device nr. 3.

In order to obtain good results for coastal protection, l/L_p should be around 1.20. Furthermore, the tested farm layout can be considered as a basic module to be repeated along the cross-shore and long-shore directions. For instance, by repeating two times this module, the mean transmission coefficient $K_{T,m}$ behind the farm would be 0.83 (it is assumed $K_{T,m}=K_{T4}^2$). If the module is repeated three times, $K_{T,m}$ would be 0.75.

Figure 9 shows that wave transmission coefficients K_T derived for the single device and for the line/s of the farm do not significantly depend on the wave steepness s_p. The scatter of the data is high, especially for K_{T2} and K_{T4}.

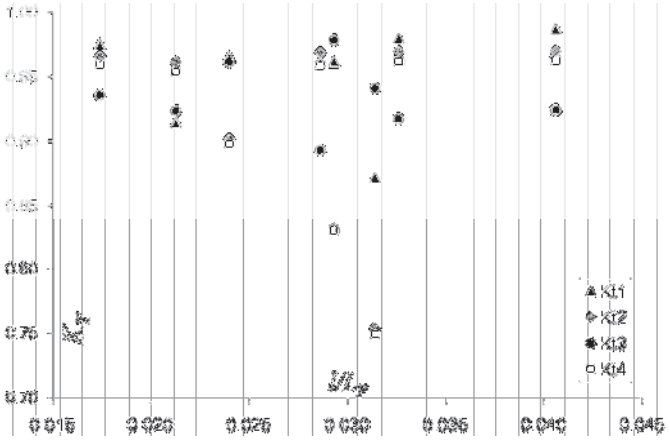

Fig. 9 – K_{T1}, K_{T2}, K_{T3} and K_{T4} against s_p.

B. Wave field in the wake of devices

The previous paragraph has shown that for a complete assessment of wave transmission behind the wave farm, wake effects have to be investigated in order to provide more accurate values of the local wave heights to be used in the estimate of K_T.

Figure 10 shows the wave field behind the second line of the farm, in terms of H_s as function of the distance from the device axis (and basin axis), for every WS. The values of H_s are obtained from time-domain analysis carried out at WGs nr. 22, 25, 26 and 27 (in this order, see Fig. 5).

The wave height in the device wake is strongly dependent on the distance from the device axis. In particular, H_s at the WG nr. 22 is affected by radiated waves, which are generated

by the model during its heaving motion. This phenomenon is more evident for higher WSs (where higher value of H_s is exactly in line with the model axis). For lower WSs (nr. 1 and 2), since the device motion is very limited, the value of H_s at the WG nr. 22 is not too much affected by generated waves.

Figure 11 also shows the zone behind the device which is affected by the wake effects. For less energetic WSs, when the device motions are small, the wake zone ends at around one device length ($1.10 \cdot l$) from the device axis, being the values of H_s at the WGs nr. 26 and 27 almost equal. For more energetic WSs instead, H_s at WGs nr 26 and 27 significantly changes (with exception of the WS nr. 8).

In conclusion, the wave field on the wake of the device is heavily affected by its heaving motions, leading to variations of the local values of the wave heights and consequently also the local intensity of wave transmission.

C. Interaction between devices

The description of the modified wave field in the gap of the first farm line allows to assess the mutual interaction between the models.

Values of H_s at WGs nr. 14 - 21 are plotted in Fig. 12 against the distance from the basin axes (both in full scale).

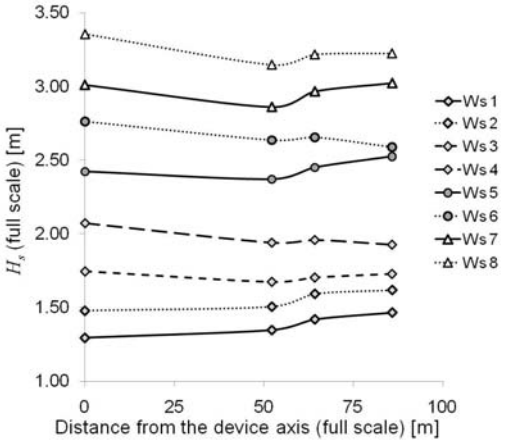

Fig. 10 –Wake effects behind the second line of the wave farm. Wave heights measured at WGs 22, 25, 26, 27.

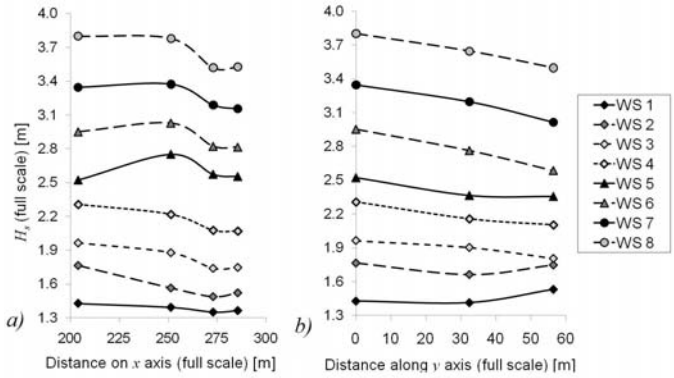

Fig. 11 – *a)* Wave field along x axis (cross-shore) and *b)* wave field along y axis (long-shore) in the gap.

The cross-shore variation of H_s along the x axis for every WS, starting from the middle of the gap (WG nr. 18, aligned with WGs nr. 19, 20 and 21) till the device closer to the shore is shown in Fig. 10.*a*. The long-shore variation of H_s instead, starting from the y axis origin (WG nr. 18, aligned with WGs nr. 15 and 17) till the device nr. 1 is plotted in Fig. 10.*b*.

It can be observed that wave heights tend to decay both along x and y axis and such tendency is more pronounced for more energetic WSs.

A constructive wave interaction between the devices in the first farm line can be noticed (see Fig. 11.*a* and 10.*b*). Such interaction is also remarked by Tab. IV, where the ratios between H_s derived from the WGs nr. 8 (H_{sWG8}) and 18 (H_{sWG18}) are reported. In the same table, the ratios between H_{m0} at the Arrays nr. 4 (H_{m04}) and the Array nr. 1 (H_{m01}) are also shown. H_{sWG8} is always lower than H_{sWG18} with exception of the two lower WSs, i.e. when the device motions are not so large.

In Fig. 11.*a* it can be also observed a significant decrease of H_s from the WG nr.19 to the WGs nr. 20 and 21. The superposition of the device wakes leads to a destructive wave interaction behind the first line, just in the zone facing the device nr. 3. This interaction entails that H_{m04} is significantly lower than H_{m01}.

The ratios H_{m04}/H_{m01} can be also assumed as the coefficient which describes the diffraction at the farm gap.

TABLE IV
RATIOS BETWEEN H_{sWG8} AND H_{sWG8} AND BETWEEN H_{m04} AND H_{m01}

	H_{sWG8}/H_{sWG18}	H_{m04}/H_{m01}
1	1.31	0.73
2	1.02	0.80
3	0.96	0.89
4	0.94	0.96
5	1.02	0.97
6	0.91	0.97
7	0.94	0.97
8	0.95	0.97

Fig. 11.*b* also remarks that the constructive wave interaction is more pronounced for more energetic attacks. For WSs 1, and 2, the device motions are such that there is not a significant increase of H_s at the WG nr. 18. In the other cases, H_s decreases approaching the device nr. 1.

The constructive wave interaction in the gap, as well as the diffraction effects behind the devices in the first line, are strongly correlated to the gap width, whose value is around 8 times the device width b. A significant reduction of H_{m04} can be achieved with the current value of gap width, but H_{m04} may further decrease by reducing the gap width up to the minimum required distance among the devices.

Visual observations of the models under testing suggested that maximum device displacements along y axis were not greater than $0.5b$ (on both sides), therefore the safe distance to be kept among the devices is around $3b$. If such distance is adopted as the gap width - assuring that there are no problems for the correct functioning of the mooring systems - the effects due to the superposition of the device wakes can provide a greater reduction of H_{m04}. This phenomenon is surely useful

for coastal protection purposes, but reduces at the same time the energy incident the device nr. 3 and thus the energy production at the second line of the farm. Therefore it would be more convenient to place the device nr.3 in a zone where the diffraction effects do not lead to a destructive wave interaction, i.e. it should be aligned with the devices composing the first line. In this way, a combined solution for coastal protection and energy production can be achieved, being the wave energy which approaches the second farm line still sufficiently high to be converted in electric energy and the wave height in the gap reduced by the hydrodynamic interaction among the devices.

D. Wave reflection

The wave reflection in front of the models can be synthetically expressed through the reflection coefficient

$$K_R = \frac{H_R}{H_I} \qquad (2)$$

where H_I is the significant incident wave height H_{m0} and H_R is the significant reflected wave height.

The reflection coefficients K_{R1} and K_{R2} are respectively evaluated at the Arrays nr. 2 and nr. 4. The dependence of these coefficient on l/L_p is shown in Fig. 11.

In general a modest fraction of the incident wave energy is reflected by the device, being K_R always lower than 0.30 (the average values of K_{R1} and K_{R2} are respectively 0.30 and 0.29).

The trends of K_{R1} and K_{R2} almost linearly increase with increasing l/L_p and the greater the l/L_p the smaller the differences between K_{R1} and K_{R2}.

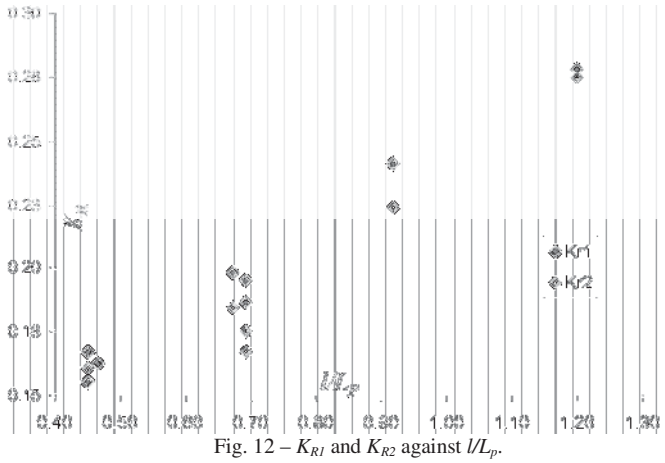

Fig. 12 – K_{R1} and K_{R2} against l/L_p.

VIII. Results for 1:30 scale tests

A. Transmission coefficient

Tab. V reports the values of K_T for every WS. H_I and H_T are the values of H_{m0} derived through the BDM analysis from the front and the back WGs Arrays respectively.

A great amount of the wave motion is transmitted behind the device, being K_T always in the range $0.80<K_T<0.86$. The mean value of K_T is determined through a weighted average based on the off-shore incident wave power and equals 0.83.

Figure 13 shows that K_T is considerably affected by l/L_p (the values of L_p are derived by the BDM analysis on the front WGs Array). More precisely, K_T increases up to reach its maximum when l/L_p equals 0.73, then it decreases to around 0.80.

TABLE V
K_T FOR DIFFERENT WSs

WS	K_T	WS	K_T
1	0.81	**6**	0.82
2	0.84	**7**	0.84
3	0.80	**8**	0.83
4	0.82	**9**	0.86
5	0.85	**10**	0.81

Good values of K_T for coastal protection purposes can be achieved when l/L_p is around 0.50 or 1.20 (K_T~0.80). In such conditions, the device does not move a lot compared to when l/L_p=0.73. In fact, from previous studies on DEXA [12], it has been shown that when l/L_p~0.73 the produced power is maximum being the device motions very large. Therefore it can be concluded that a strong correlation among the device displacements and wave transmission exists and the greater the device motions the higher the wave transmission.

Finally, K_T does not depend on the wave steepness s_p, see Fig. 14 where the data show a lot of scatter.

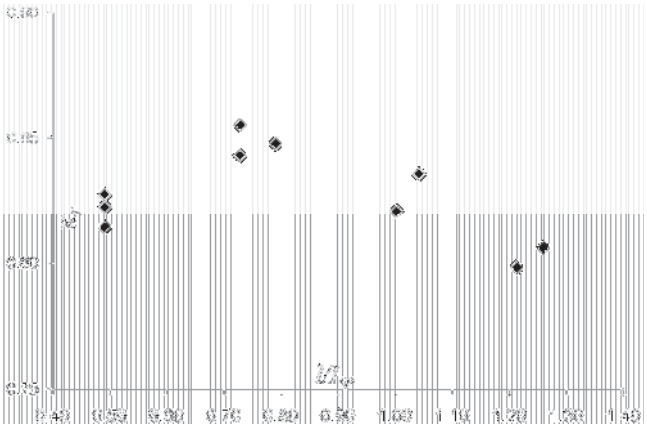

Fig. 13 – K_T against l/L_p of the big model.

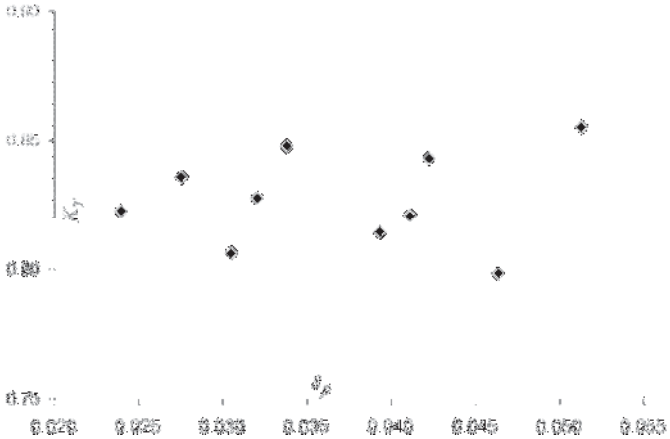

Fig. 14 – K_T against s_p for the big model.

B. Wave field in the wake of the device

In order to describe the wave field in the wake of the device, Figure 15 shows the values of significant wave heights H_s. measured at WGs nr. 8, 7, 14 and 16 against the distance from model axis, for every WS.

For the WSs nr. 1, 2, 3, 4, since the model does not move a lot, values of H_s in line with the device are not affected by the radiated wave field and the highest values of H_s are found at the farthest point of the wake, whereas significant changes in H_s at WGs nr. 8 and 7 can be observed for more energetic WSs.

The values of H_s at the WGs nr. 14 and 16 are almost equal for every WS, therefore it can be concluded that the wake zone extends at most to $0.63 \cdot l$ from the device axis.

In conclusion, also for the big DEXA model, the wave field in the wake strongly depends on the radiated waves, generated by the heaving motions of the device.

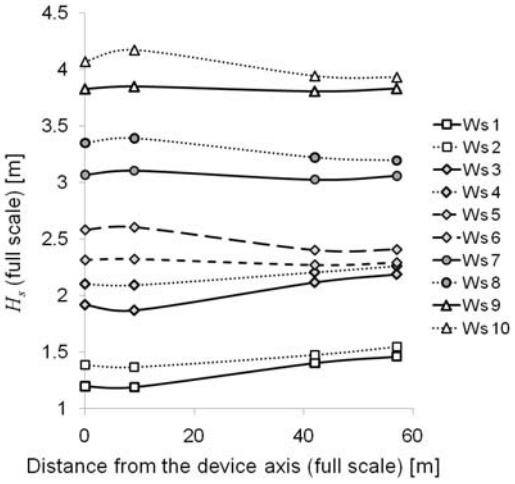

Fig. 15 –Wake effects behind the 1:30 scale model.

C. Changes in wave direction

In order to verify the importance of the device motion for wave transmission, in this paragraph changes in wave direction behind the DEXA are evaluated. Such variations are represented by means of $\Delta\theta$ that is defined as follows:

$$\Delta\theta = \theta_I - \theta_T \qquad (2)$$

where θ_I and of θ_T are computed by means of the BDM analysis of the measurements gained from front and back WGs arrays, respectively.

An example of BDM analysis of the WS nr. 2 for defining directional wave spectra is given Fig. 16. Detailed values of θ_I and of θ_T for every WS are provided in Tab. VI.

The values of $\Delta\theta$ in Fig. 17 show significant changes in the transmitted wave directionality (up to 2.90°) and the comparison between Figures 12 and 16 shows that $\Delta\theta$ is greater when $0.50<l/L_p<1.20$, i.e. when the values of K_T are high. In addition, from the same comparison it can be noticed that when l/L_p is around 0.50 or 1.20, $\Delta\theta$ is low (<1°). The maximum value of $\Delta\theta$ is achieved for WS nr.2, where $l/L_p=1.04$ ($K_T=0.84$, one of the highest recorded values of the transmission coefficient).

In conclusion, the changes in the transmitted wave directionality are strongly correlated to the device motions around its rest position: when $\Delta\theta$ is high the device movements are large and thus also the transmission coefficient tends to increase.

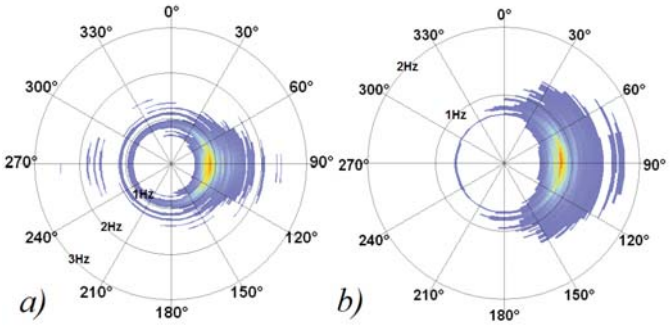

Fig. 16 –Incident (15.*a*) and transmitted (15.*b*) directional spectra for the WS nr. 2.

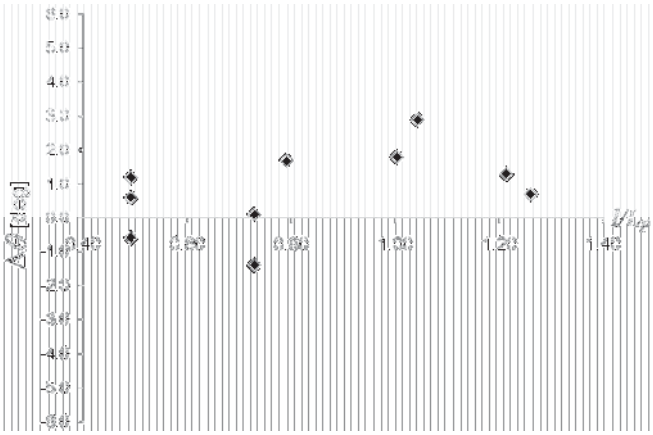

Fig. 17 –Variation of wave directions behind the model against l/L_p.

TABLE VI
θ_I AND θ_T FOR DIFFERENT WSS (WAVE ATTACK AT 90° BEING PERPENDICULAR TO THE BEACH).

WS	θ_I [°]	θ_T [°]
1	90.7	90.00
2	92.6	89.70
3	90.9	89.60
4	90.8	89.00
5	91.0	89.30
6	88.6	89.20
7	89.5	90.90
8	91.9	90.70
9	90.9	90.80
10	91.4	90.80

D. Wave reflection.

The reflection coefficient, whose values are summarised in Table VII for each WS, vary in a quite small range ($0.20<K_R<0.32$). A small fraction of wave is reflected in front of the device, being K_R always lower than 0.35 (the mean value is 0.25).

The values of K_R in Fig. 18 are quite affected by l/L_p and show a totally opposite trend compared to K_T. The minimum

values of K_R are achieved in the range $0.70 < l/L_p < 0.80$, when a greater fraction of wave motion is transmitted behind the device.

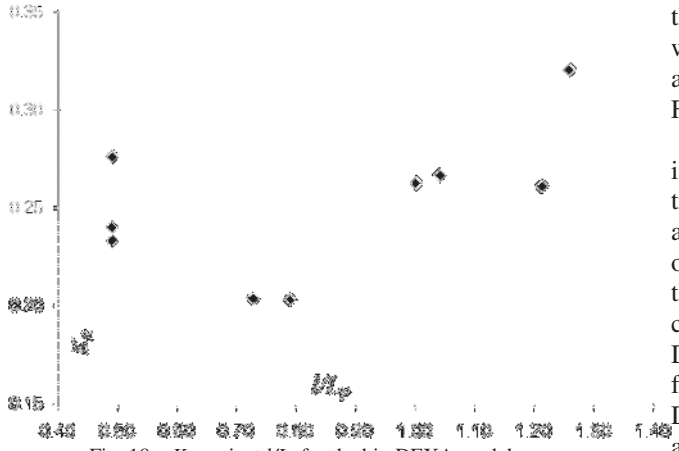

Fig. 18 – K_R against l/L_p for the big DEXA model.

TABLE VII
VALUES OF K_R FOR THE BIG DEXA

WS	K_R	WS	K_R
1	0.321	**6**	0.276
2	0.267	**7**	0.204
3	0.261	**8**	0.233
4	0.263	**9**	0.204
5	0.203	**10**	0.240

IX. SCALE EFFECTS

A. *Wave transmission*.

Hereafter, values of K_T from tests in 1:60 and 1:30 scales are compared. For the first ones, the values of K_{TI} are considered, being the transmission coefficient referred to a single device within the farm. For convenience, it is recalled as $K_{T1:60}$, whereas $K_{T1:30}$ stands for the transmission coefficient derived from 1:30 scale tests. Such values are plotted in Fig. 18. It can be noticed that:

$K_{T1:60}$ is always higher than $K_{T1:30}$, although their trends are quite similar: they increase with increasing l/L_p, up to reach their maxima when $l/L_p = 0.72$ ($K_{T1:60}$=0.99 and $K_{T1:30}$=0.86), then, from such point, they decrease. $K_{T1:60}$ in Fig. 18 seems to be simply shifted upwards compared to $K_{T1:30}$ and their values differ on average of 0.12. Differences are greater for low values of l/L_p and tend to reduce with increasing l/L_p.

The ratios h_I and h_T between H_I and H_T for 1:30 and 1:60 scale tests are respectively defined as:

$$h_I = \frac{[H_I]_{1:30}}{[H_I]_{1:60}} \quad (3)$$

$$h_T = \frac{[H_T]_{1:30}}{[H_T]_{1:60}} \quad (4)$$

h_I is always greater than h_T, see Tab. VIII. Based on the values reported in this table, it can be observed that the differences among K_T in Fig. 19 (i.e. $K_{T1:60} > K_{T1:30}$) are essentially due to differences among h_I and h_T for each WS: the greater the differences among h_I and h_T the greater the differences among $K_{T1:60}$ and $K_{T1:30}$. The variation between H_I and H_T in the two scales for the same test may be explained by the wavemaker typical range of wave generation (particularly water depth) and by the different types of data analysis adopted (the BDM for 1:30 scale tests and the Mansard and Funke's method for 1:60 scale tests).

Another important aspect to be accounted for is the model inertias, which affect the device mobility and thus the wave transmission. The device weights for 1:30 and 1:60 scale tests are not perfectly scaled, as well as the weight per unit length of the mooring chains. In full scale, the big model is heavier than the small one: the total weight (device+mooring) in static conditions (see Fig. 5) is $1.00 \cdot 10^6$ kg whereas for the small DEXA it is $0.85 \cdot 10^6$ kg. Under the higher WSs, i.e. when the front chains tend to be totally raised from the floor, the big DEXA is still heavier than the small one (their total weights are respectively $1.09 \cdot 10^6$ kg and $0.91 \cdot 10^6$ kg).

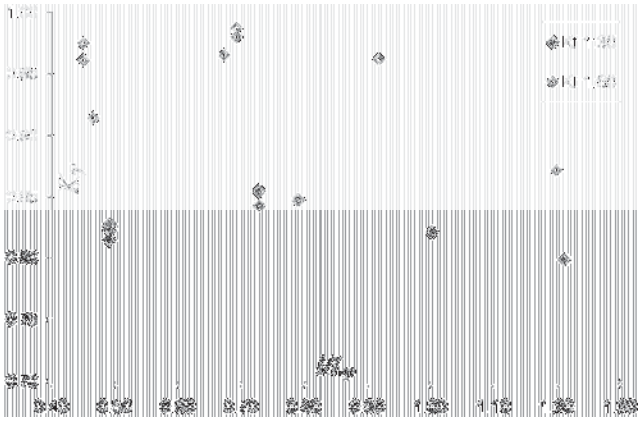

Fig. 19 – Comparison among K_T values at different scales.

From the comparison, a heavier system provides better results for coastal protection, being $K_{T1:30}$ lower than $K_{T1:60}$. In other terms, the lighter the system the greater the delay of the device in coming back to the rest position, leading to a significant increase of wave transmission.

TABLE VIII
h_I AND h_T, DERIVED FROM TESTS AT DIFFERENT SCALES

WS	h_I	h_T	WS	h_I	h_T
1	1.26	1.15	**5**	1.33	1.14
2	1.36	1.16	**6**	1.34	1.22
3	1.31	1.15	**7**	1.30	1.13
4	1.35	1.14	**8**	1.33	1.13

The lower mobility of DEXA in 1:30 scale is confirmed by a smaller wake zone ($0.63 \cdot l$ from the device axis) compared to the wake obtained for 1:60 scale tests ($1.10 \cdot l$).

B. *Wave reflection*

In the following paragraph, reflection coefficients for tests in 1:60 scale ($K_{R1:60}$) and for the ones in 1:30 scale ($K_{R1:30}$) are compared. From such comparison, it can be stated that wave

reflection from the big DEXA model is higher than from the small ones.

As for the transmission coefficient, it is possible to define the ratio between H_R derived from 1:30 and 1:60 scale tests:

$$h_R = \frac{[H_R]_{1:30}}{[H_R]_{1:60}} \quad (5)$$

The values of h_R are reported in Tab. IX. By comparing the results in Tab. IX with Tab. VIII it can be observed that h_R is higher than h_I. It means that H_R is greater for the big model than for the small one, leading to higher values of $K_{R1:30}$.

It is worthy to remark that trends of $K_{R1:30}$ and $K_{R1:60}$ differ a lot when l/L_p is low (<0.70), i.e. when the device is allowed to large movements. In these cases, the differences in the $K_{R1:30}$ trends can be explained by the inertia effects induced by the different weights of the tested devices.

TABLE IX
h_R DERIVED FROM TESTS AT DIFFERENT SCALES

WS	h_R	WS	h_R
1	1.18	**5**	1.45
2	1.48	**6**	1.93
3	1.34	**7**	1.36
4	2.24	**8**	2.06

X. CONCLUSIONS

Tests were carried out in the Aalborg wave basin to examine the hydrodynamics around a wave energy farm composed by f-WECs named DEXA, reproduced in 1:60 scale. These tests were integrated with hydrodynamic measurements on a bigger DEXA model in 1:30 scale.

Results show that wave transmission is high, being K_T always greater than 0.75 and the presence of the device along the second farm line does not produce a significant effects if compared with the first farm line.

The distribution of wave heights H_s behind the device is strongly affected by heaving motions and the extent of the wake zone can significantly change with varying the WS (larger wake zones are achieved for more energetic WSs). Transmission coefficients K_T strongly depend on the device to wave length ratio l/L_p: in the tests performed with multiple devices the values of K_T decrease with increasing l/L_p The model length is therefore the most important design parameter to be tuned on the basis of the wave climate at the selected installation site.

The values of K_T also suggest that the adopted farm module should be repeated along the cross-shore direction at least three times in order to provide a combined solution for reducing the wave motion (K_{Tm}= 0.75) and for maximising the energy production.

To further minimise K_T without compromising energy production, the farm layout can be also optimised. The gap width should be reduced up to the minimum required distance (3*b*), in order to benefit from the device interaction, and the devices in the back line should be aligned to the ones in the first line.

Furthermore, the inertia effects on the device mobility affect both wave transmission and wave reflection, K_T and K_R: if other design features are kept constant, a heavier system (device + mooring) gives better result for reducing H_I.

The comparison of wave heights obtained in the basin suggests that – a part from different methodologies adopted in data processing- scale effects are mainly induced by the conditions of wave generation with respect to the limitations of the wavemaker.

ACKNOWLEDGMENT

The support of the European Commission through FP7.2009-1, Contract 244104 - THESEUS project ("Innovative technologies for safer European coasts in a changing climate"), www.theseusproject.eu, and the support of the Danish Council for Strategic Research through SDWED project (Structural Design of Wave Energy Devices), www.sdwed.civil.aau.dk, are gratefully acknowledged.

REFERENCES

[1] Martinelli L., P. Ruol, B. Zanuttigh, (2008): *Wave basin experiments on floating breakwaters with different layouts*, Applied Ocean Research, 30, 199-207.

[2] Kofoed, J. P (2009): *Hydraulic evaluation of the DEXA wave energy converter*. DCE Contract Report No. 57. Dep. of Civil Eng., Aalborg University, Apr. 2009.

[3] Nørgaard J. H., Poulsen M., *Wave height reduction by means of wave energy converters*, MSc in Civil Engineering, 4th. Semester, Aalborg University

[4] Beels C., Troch P., De Visch K., Kofoed J.P., De Backer G., (2010), *Application of the time-dependent mild-slope equations for the simulation of wake effects in the lee of a farm of Wave Dragon wave energy converters*, Renewable Energy, Volume 35, Issue 8, August 2010, Pages 1644-1661

[5] Aalborg University, 2007. AwaSys homepage. http:// http://hydrosoft.civil.aau.dk/AwaSys

[6] Hald, T., Frigaard, P., (1997), *Alternative Method for Active Absorption in Multidirectional Waves*. Proc. IAHR Seminar on Multidirectional Waves and Thri Interaction with Structures, San Francisco, Aug. 1997

[7] Harris R.E., Johanning L., Wolfram J., (2004), *Mooring systems for wave energy converters: A review of design issues and choices*, Heriot-Watt University, Edinburgh, UK.

[8] Esmailzadeh E., Goodarzi A., (2001), Stability analysis of a CALM floating off-shore structure, International Journal of Non-Linear Mechanics 36 (2001) 917}926

[9] Aalborg University, 2007. WaveLab 2 homepage. http://www.hydrosoft.civil.auc.dk/wavelab.

[10] Hashimoto N., Kobune, K., (1988), Estimation *of directional spectrum from a Bayesian approach*. Proc.21st ICCE Vol 1. ASCE pp.62-72

[11] Mansard E.P.D, Funke E.R., (1980), *The measurement of incident and reflected spectra using a least squares method.* Proc. of the 17th Int. Conf. on Coastal Engineering.

[12] Zanuttigh B., Martinelli L., Castagnetti M, Ruol P., Kofoed J.P., Frigaard P, (2010) *Integration of wave energy converters into coastal protection schemes*, 3rd International Conference on Ocean Energy (ICOE), 6 October, Bilbao